Indian Journal of Chemistry
Vol. 63, June 2024, pp. 543-556
DOI: 10.56042/ijc.v63i6.7542

Some pyridyl moiety based metal complexes (*viz*., Mn^{+2}, Co^{+2} and Zn^{+2}) as potential anticancer agents and DNA nucleobase interaction: A DFT approach

Benzir Ahmed[a], Pratyashee Barukial[a], Basanta Singha[b], Upasana Bora Sinha[b] & Bipul Bezbaruah*[a]

[a] Department of Applied Sciences, Gauhati University, Guwahati 781 014, Assam, India

[b] Department of Chemistry, Nagaland University, Lumami 798 627, Nagaland, India

E-mail: bipulbezbaruah@gmail.com

Received 25 December 2023; accepted (revised) 24 May 2024

Many experimental evidences reveal that a new set of complexes involving transition metals (*viz*., Mn^{+2}, Co^{+2} and Zn^{+2}) with pyridyl moiety ligands are being investigated as potential anticancer agents due to their intense ability to follow intercalation mechanisms with DNA nucleobases. Although, the interaction mechanism between anticancer agent-DNA nucleobase itself is quite complicated to understand by using conventional techniques; but some computational methods may still be very helpful for analyzing the proper binding mode of interaction. Hence, exploring the favoured interaction sites within an anticancer agent and finding its donor-acceptor ability is really a challenging task. Moreover, for any drug-DNA receptor complex; there must be few changes in their electron charge density, structure of the molecule, chemical reactivity parameters, *etc*. DFT is one of the best known and most affordable methods for investigating such exploration in metal complexed anticancer agents. Herein, we have described an attempt to investigate the interaction mechanism of some pyridyl moiety based Mn^{+2}, Co^{+2} and Zn^{+2} metal complexes as potential intercalating anticancer agents by using computational techniques.

Keywords: Pyridyl moiety, Anticancer agent, DFT, DNA, Metal complex

Novel transition metals-based anticancer agents have gained significant interest in recent years, as metal ions directly coordinate with the ligands *via* donor atoms such as -O, -N and -S in a precise 3D structure, which may allow the molecule be able to recognize, design and potentially interact with the specific receptors[1-4]. Hence, the effectiveness of metal-based anticancer agents depends on their chemical structures and donor-acceptor behaviour as interacting ligands. Some of the transition metal complexes show effective pharmacological behaviours *i.e*., antibacterial, antifungal, anticonvulsant, antidiabetic, anti-inflammatory, antioxidant and antiproliferative/ antitumor activities[5-8]. Specially, metallic compounds other than *cis*-platin have long been a target of interest for researchers, as they are said to be the most effective and best known anticancer metallodrugs[9,10]. Due to their potential antiproliferative action, higher thermodynamic stability in aqueous phase and flexibility to change their oxidation states to the biological target sites, the development of physiologically active metallodrugs with endogenous metal ions has drawn a lot of interest[11-13]. However, *in vivo* interaction mechanism of such metal complexes within the possible target sites, *viz*., proteins and nucleic acids is still poorly known; *e.g*., some of the bio-active transition metal complexes containing an antibacterial drug flumequine reveal that they directly interact with nucleobases and serum albumin[14-19]. The pyridyl moiety or N-based pyridyl ligands with transition metals have recently been extensively studied as potential anticancer agents; *e.g*., Pd, Ru, Rh, Cu, La, *etc*. metal complexes with pyridine, imidazole along with 1,10-phenanthroline ligands; and their derivatives are showing promising antitumor properties in regard to drug design research[20]. Again, metal complexes comprising pyridyl or polypyridyl ligands are largely dependent on the nature, geometry and overall arrangement of the coordinated ligand. In particular, due to their electron-deficient nature, N-based heterocyclic rings are excellent π-electron acceptors to form a favourable donor-acceptor complex, which results in smooth intercalation of such aromatic rings into DNA base pairs[21-23]. Additionally, a typical tridantate ligand, di(picolyl) amine (DPA) can form stable complexes with transition metal ions by strongly coordinating with their metal cations and using two pyridine nitrogens

as well as an amine nitrogen[24]. Similarly, the norharmane ligand *i.e*., 9H-Pyrido[3,4-b]indole often known as Hnor, is an alkaloid of the β-carbolines (βCs) family containing fused rings; which exhibits a variety of pharmacological and anticancer properties as well as inhibition of DNA topoisomerase I and II, *etc*.[25-27] A remote hydrogen-bond donor group exist in Hnor, which may favour to coordinate with metal ions to show affordable non-covalent interactions[28-31]. Literature reveals that metal complexes, *viz*., Mn^{+2}, Co^{+2} and Zn^{+2} ions are significant; as they are involved as cofactors in various enzymes in any biological system. These metal-based complexes have been developed as anticancer agents due to their significantly less toxic nature and potential application as photosensitizers in photodynamic therapy[32].

In our current study, we have selected some of the pyridyl moiety based Mn^{+2}, Co^{+2} and Zn^{+2} metal complexes as novel anticancer agents with experimentally measured half-maximal inhibitory concentrations *i.e*., IC_{50} values; later, quantum mechanical investigation was carried out to analyze their binding mechanism with DNA nucleobases. We have also analyzed the effect of N-based pyridyl ligands such as 2-di(picolyl)amine-N-(quinolone-8-yl)acetamide (L1), Pyridine (L2) and 9H-Pyrido[3,4-b]indole or norharmane (L3) with selected transition metal-based complexes *viz*., Dichloro-2-Di(picolyl)amine-N-(quinoline-8-yl)acetamide-manganese(II) (A1), Bis(5-chloroquinolin-8-olato)-bis(pyridine)-cobalt(II) (A2) and 9H-Pyrido[3,4-b]indole-1,10-phenanthroline-bis(nitrate)-zinc(II) (A3) within the DNA nucleobases. Herein, some of the pyridyl moiety ligands such as L1, L2 and L3 with Mn^{+2}, Co^{+2} and Zn^{+2} based metal complexes (*i.e*., A1, A2 and A3) are considered as possible metal-based anticancer agents for our study (Table 1). Additionally, the computed interaction energy results may be justified by analyzing the Natural Bond Orbital (NBO), which shows changes in electronic transition that occurs during the anticancer agents and DNA nucleobase interaction. Moreover, other molecular visualization and analysis programs such as NCI, VMD, ELF, BSA and ESP were also carried out for the selected anticancer agents-DNA base pair stacked models; which help in visualizing the possible interacting sites, changes in molecular conformation and electronic densities present in the M^{+n} ions.

Methodology

Computational analysis

As the experimental binding constant is very difficult to calculate *in vivo*; hence, in our case we have computed only the short/long range van der Waal interaction without any binding constant value[33]. Density functional theory (DFT) is usually the most competent technique to investigate the weak molecular interaction such as dipole-π, ion-π, π-π and so on. The DFT formalism was applied to carry out the optimization of molecular geometries with the help of Gaussian G16 A.01 software. Here, the most frequently used global hybrid generalized gradient approximation *i.e*., B3LYP functional approach with additional keywords "empirical dispersion = gd3bj" was used in the input files of molecular geometry[34]. After optimizing all of the selected metalated complexes and AT/GC base pairs, the geometries were utilized to construct the required stacked systems. All the stacked models were prepared with the help of GaussView5.0 and quantum chemical calculations were processed using Gaussian16 program code[35].

Mulliken charge (MC) analysis is a prominent computational technique which is used to determine the distribution of electron charges among individual atoms of a molecule[36,37]. The calculation of MC is essential as it enables the determination of electron populations attributed to each atom, which offers valuable insights into electron density and bonding characteristics within the molecular system. Again, NBO (Natural Bond Orbital) analysis provides a

Table 1 — IUPAC names and IC_{50} values of some metal-based complexes with pyridyl moiety as anticancer agents

Anticancer agents	IUPAC Names/molecular formula	Interacting ligand	IC_{50} Values(μM)
A1	Dichloro-2-Di(picolyl)amine-N-(quinoline-8-yl)acetamide-manganese(II) $[Mn(QA)Cl_2]$	L1	11.03
A2	Bis(5-chloroquinolin-8-olato)-bis(pyridine)-cobalt(II) $[Co(HClQ)_2(Py)_2]$	L2	7.04 ± 0.06
A3	9H-Pyrido[3,4- *b*]indole-1,10-phenanthroline-bis(nitrate)-zinc(II) $[Zn(Hnor)(Phen)(NO_3)_2]$	L3	1.26 ± 0.07

detailed description of the bonding interactions in a molecule by analyzing the electron density distribution. These NBOs are used to understand the nature and strength of chemical bonds, lone pairs and other electron density features in a molecule. It also evaluates donor-acceptor behaviour, inter-molecular interactions and intra-molecular charge transfer mechanisms[38]. Again, other physicochemical properties may be responsible for the transfer of electric charges and structural stability of stacked complexes[39-41]. On the other hand, the probable interacting regions between anticancer agents-DNA nucleobase stacked system can be analyzed by using different molecular visualization and analysis techniques such as MEP, NCI, VMD, ELF, BSA and ESP[42,43]. The Multiwave functional Analyzer software is extremely useful tool for this analysis which helps in prediction of the most favoured interacting sites between an anticancer agent-DNA nucleobase complexes[44]. Moreover, for any molecular counterpart the variation of electron cloud density during molecular interaction can effectively investigated by studying their chemical bond analysis *i.e.*, electron localization function (ELF) with localized orbital locator (LOL) plots[45,46]. Molecular surface analysis techniques *viz.*, Electrostatic Potential (ESP) and Becke Surface Analysis (BSA) were also carried out for the prediction of possible active electrophilic and nucleophilic sites. Meanwhile, in order to reveal molecular interactions such as hydrogen bonding and van der Waals (vdW); BSA was performed by using the Multiwave function software[47-49].

Structural analysis

Theoretical analysis reveals that the interaction mechanism of an intercalating anticancer agents and DNA nucleobases may always occur through a common non-covalent π-π interaction. Usually, in bio-active metal-based anticancer agents, there exist various interacting sites; however, in our case, we specifically focus on the most active intercalating sites. For evaluating the *in vivo* compatibility of drug-DNA interactions involving non-covalent binding, a favoured intermolecular separation of 3.6Å was applied to all anticancer agent-DNA nucleobase stacked complexes[50]. Further, the π-π interaction of metalated agents and DNA base pairs has been analyzed, where these agents are positioned over AT/GC base pairs. Therefore, all the stacked models have been analyzed to determine the probable interaction energy between anticancer agents-DNA nucleobases (Fig. 1)[51].

Results and Discussion

Comprehensive analysis of metal-based anticancer agent with AT/GC base pair complexes

In our study, some pyrazinyl moiety based Mn^{+2}, Co^{+2} and Zn^{+2} metal complexes are selected as potential anticancer agents, which are displayed in Table 1 and Fig. 1. The primary objective for selecting these metalated complexes as they contain at least one N-based aromatic ligand; which is known for its strong compatibility with DNA nucleobases. For all the selected metal-based agents, a comprehensive analysis of their stacking interactions has revealed a highly favourable binding affinity with the base pair, which is evident from the most negative interaction energy (I.E.) values, as displayed in Table 2. In computational calculations, a greater negative value for the interaction energy of a molecular complex indicates a more stable conformation.

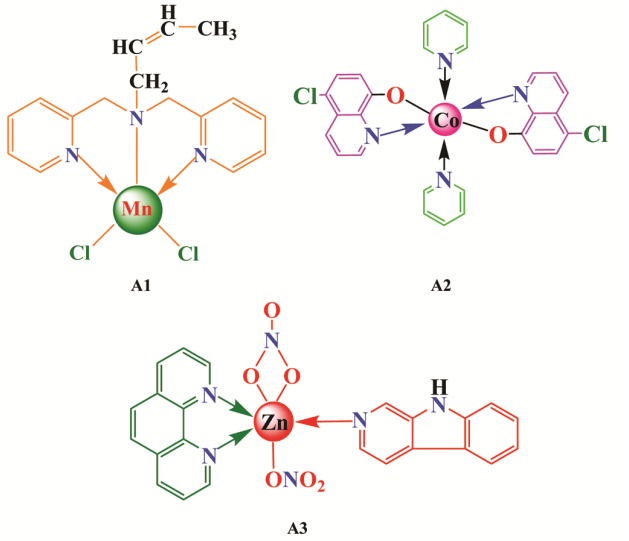

Fig. 1 — Optimized structures of pyridyl moiety based Mn^{+2}, Co^{+2} and Zn^{+2} metal complexes (A1, A2 and A3)

Table 2 — Minimized stacked interaction energy (kcal/mol) for *pyridyl moiety* metal based anticancer agents with AT/GC base pairs of DNA nucleobases

Anticancer agents	Interaction energies (kcal/mol)	
	AT	GC
A1	–10.63	–8.45
A2	–16.26	–19.58
A3	–22.08	–25.56

The I.E. calculations reveal the sequence of stability among the stacked systems of metalated agents-AT/GC base pair complexes as indicated by their calculated interaction energy values, which are shown below:

For AT stacked complex: A1 < A2 < A3

For GC stacked complex: A1 < A2 < A3

Based on the observed sequence of stability among the metalated anticancer agents, it is evident that anticancer agent, A3 *i.e.*, [Zn(Hnor)(Phen)$(NO_3)_2$] exhibits a significantly higher favoured and effective binding affinity with DNA nucleobases; which is due to the more negative values of interaction energy *i.e.*, –22.08 kcal/mol and –25.56 kcal/mol in both AT and GC stacked systems respectively (Table 2). Interestingly, Mn-based anticancer agent (A1) *i.e.*, [Mn(QA)Cl_2] also observes a significant characteristic, as it exhibits the least stable and most repulsive AT and GC stacked conformation, which has the least negative interaction energy values *i.e.*, –10.63 and –8.45 kcal/mol; when compared to its counterparts displayed in Table 2. Further, A2 complex also exhibits consistently negative interaction energy values which closely follow the A3 complex. However, anticancer agent A1 represents the lowest negative interaction energy value, which indicates unstable stacked conformations both in AT and GC base pairs (Table 2). These observations collectively suggest that stacked A3-AT/GC complex results relatively higher negative interaction energies both in AT & GC interactions in comparison to other metal-based anticancer agents. Additionally, the interaction energy calculations for these stacked configurations consistently reveal higher negative I.E. values, suggesting that it may occur due to the presence of significant non-covalent interactions within these agent-DNA systems.

The theoretical analysis of the interaction mechanism of the Zn^{+2}-based anticancer agent (A3) *i.e.*, [Zn(Hnor)(Phen)$(NO_3)_2$] with DNA base pairs is relatively comfortable because of the presence of bidentate nonharmane (Hnor) ligand, which is a β-carboline derivative with a fusion of two moieties of indole and pyridine; therefore, due to its planar structure, the ligand can smoothly intercalate within DNA base pairs. Again, the efficacy of such interactions is further enhanced by the addition of a remote H-bond donor group of Hnor ligand, along with the presence of a nitrate ion (NO^{3-}) as an additional ligand; where NO^{3-} anion serves a dual role by maintaining charge neutrality and offering the capacity for hydrogen bond acceptance. These potentially tridentate anionic ligand NO^{3-} can function in both monodentate and chelating forms to complete the coordination sphere of the metal. Moreover, the presence of the planar ligand *i.e.*, phenanthroline contributes to additional stability within the complex. Thus, the A3 complex is able to interact with DNA base pairs (AT/GC) more effectively than other metal-based complexes (Fig. 2).

Again, in case of A1 complex *i.e.*, [Mn(QA)Cl_2], the coordinating N-based tridentate QA ligand (2-di(picolyl)amine-N-(quinolone-8-yl)acetamide) is very bulky and non-planer, which makes the Mn^{+2} molecular complex unstable as compared to the previously studied A2 and A3 metal complexes. Hence, A1 shows a weak binding affinity with AT/GC base pairs, contributing to its overall instability in stacked configurations with A1-AT/GC systems. The effect of the Mn^{2+} ion in the A1-AT/GC minimized stacked model is evident through the changes observed in the Mulliken charge density value of Mn^{2+}, as illustrated in Fig. 3. Moreover, among all the studied metalated anticancer agents, the A2 complex, *i.e.*, [Co$(HClQ)_2(Py)_2$], shows moderate interaction with DNA base pairs. This is partly due to the planar structure of the pyridyl ligand (Py), which allows it to smoothly intercalate within AT/GC base pairs (Fig. 2 and Table 3). Additionally, the less sterically hindered structure of the HClQ ligand contributes to the stability of such stacked systems and the role of the Co^{2+} group can be observed by analyzing the changes in the MC density, as depicted in Fig. 3. Based on the above analysis of minimized stacked models of the studied agents with DNA base pairs, it was revealed that all anticancer agents preferably interact with the Adenine and Guanine bases of DNA nucleobases (Table 3). According to the interaction energy values of these stacked models, the complexes A2 and A3 are considered to be highly GC-specific in nature; as they preferentially interact with GC rather than AT base pair. The sequence-specific binding of GC-A2 & GC-A3 systems can be investigated by calculating the binding energy of these stacked complexes which results in higher negative interaction energy values *i.e.*, –19.58 and –25.56 kcal/mol as compared to the AT-A2 and AT-A3 stacked system *i.e.*, –16.26 and –22.08 kcal/mol

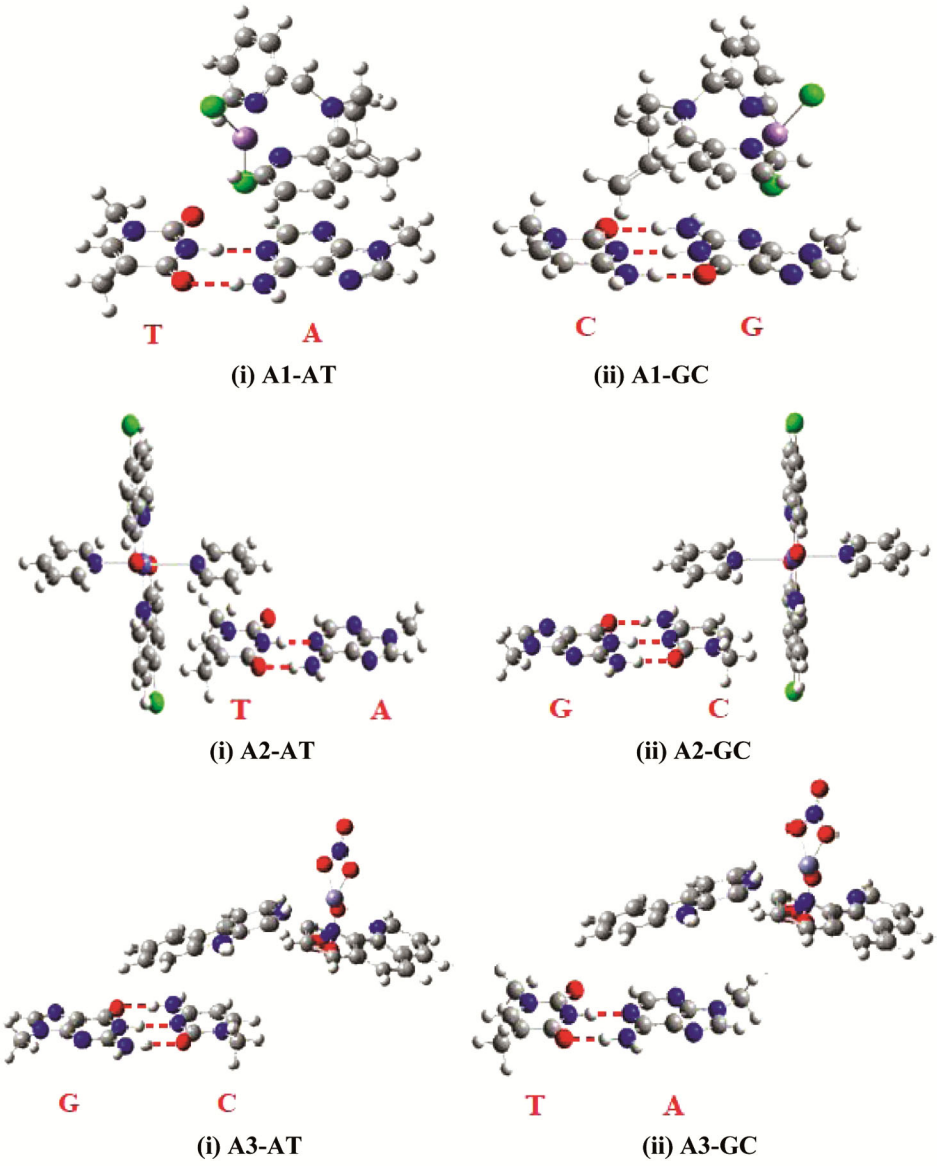

Fig. 2 — Minimized stacked models of metal-based anticancer agents (A1, A2 and A3) with AT and GC base pairs

respectively. But, the less favoured A1 stacked complex shows AT specificity with I.E. values –10.63 kcal/mol, which is displayed in Table 2. The detailed information regarding the most favoured and unfavoured binding sites of these stacked models along with their specific tendency to bind within AT/GC base pairs is clearly depicted in Table 3.

Again, the Irving-Williams series suggests that, presence of Zn^{2+} ion has a significant effect on the cytotoxicity of various transition metal complexes. This series provides insights into the relative stabilities of the studied metal ion complexes[52]. In the case of divalent ions of first-row transition metals in high-spin complexes, the stability consistent trend for complex formation is found as follows: Mn (II) < Fe (II) < Co (II) < Ni (II) < Cu (II) > Zn (II). Consequently, the bidentate ligand L3 readily coordinates with the Zn^{2+} ion which potentially leads to the most stable Zn^{2+}-L3 complex formation. This suggests that the tendency of metal ions to form complexes must follow the order: Mn (II) < Co (II) < Zn (II). In our current investigation, we have discovered that Zn^{2+}-based complexes exhibit a strong affinity for binding to DNA nucleobases.; which may further be justified by investigating the chemical reactivity parameters like hardness, softness, electron charge densities, donor-acceptor nature and non-covalent analysis to observe the proper interaction sites.

Electronic properties

Analysis of Mulliken charge (MC)

Mulliken charge is a concept in computational chemistry that refers to the distribution of electron density within a molecule, which are used to analysis chemical reactions, reactivity and the prediction of properties such as dipole moments and bond orders. They can be particularly useful in understanding the behaviour of molecules in various chemical and biological processes. The study conducted an analysis of Mulliken charge (MC) density for M^{+2} metal ions in selected anticancer agents, both in unstacked and stacked models. The aim was to observe the changes in their stacking interaction energy values and understand the effect on MC density. The results revealed significant differences in the MC density values of the stacked systems in comparison to their individual systems.

In the case of the Zn^{+2} ion in A3, the computed MC density was notably higher at 1.488, compared to 1.104 for AT and 1.099 for GC base pair systems. These variations underscore the substantial shifts in MC density resulting from the stacking interactions between these metal-containing anticancer agents and DNA base pairs. The most prominent changes in MC density values were observed in the A3-AT/GC stacked complex, which suggest the formation of highly stable stacked molecular conformation. To visually depict the relative MC density analysis of the Mn^{+2} ion both in stacked along with unstacked metalated anticancer agents, a bar graph was presented in Fig. 3. Among the GC-stacked systems, the MC calculation for the Zn^{+2} ions in the A3 complex significantly decreased from 1.488 to 1.099. This indicates a substantial transfer of electronic charge density from the Zn^{+2} group of anticancer agent towards DNA base pairs within the stacked system. Consequently, the A3-GC stacked complex exhibits stability, as evidenced by its relatively higher negative interaction energy value. In contrast, within the A1 and A2 systems, the changes in MC density for the Co^{+2} and Mn^{+2} ions in both unstacked and GC-stacked complexes were relatively small, with values of 0.264 for Mn^{+2} and 0.274 for Co^{+2}. These minor changes suggest a limited redistribution of electronic charge density from the Mn^{+2} and Co^{+2} ions to the GC base pair in a stacked system, resulting in the formation of least stable as well as less favoured stacked complexes with lower negative I.E. values (Table 2).

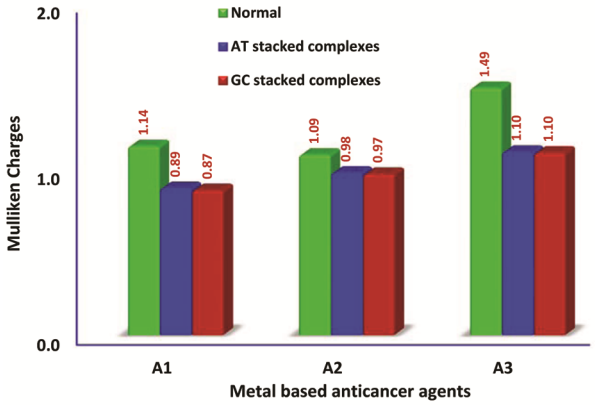

Fig. 3 — Mulliken charge distribution for Mn^{+2}, Co^{+2} and Zn^{+2} stacked and unstacked metal-based anticancer agents with AT/GC base pairs

Natural bond orbital (NBO) analysis

NBO analysis is a computational technique which provides new insights into the nature of chemical bonding, the electron distribution within molecules to understand the intermolecular interactions within a donor-acceptor complex. In the context of drug-DNA base pairs stacked systems, NBO analysis helps reveal the intriguing phenomenon of intra-molecular charge transfer (ICT). An increase in charge delocalization indicates a higher degree of conjugation within a molecular complex. This enhanced charge delocalization and conjugation contribute significantly to the stability of stacked molecular complexes. It signifies a stronger interaction and sharing of electrons between the donor and acceptor orbitals, ultimately resulting in a more stable and well-defined interaction within the complex. This concept is fundamental for understanding the electronic configuration and stability of various

Table 3 — Probable interacting sites of the *pyridyl moiety* metal-based anticancer agents and their binding specificity towards AT/GC base pairs

Anticancer Agents	Preferred Nucleobase	Base pair Specificity	Favoured Interacting sites	Unfavoured Interacting sites
A1	A and G	AT	Quinoline based ligand	–
A2	A and G	GC	Pyridyl ligand	HClQ ligand
A3	A and G	GC	Hnor ligand	Phen ligand

molecular systems. To quantify these changes, NBO analysis provides values of perturbation energy, as discussed in Table 4. The strong interaction between electron donors and acceptors is a consequence of the larger E^2 value, signifying a more extensive conjugation within the entire system. In case of the metal-based anticancer agents, the observed E^2 values during the complex formation process, which arise from internal transitions *i.e.*, charge delocalization are listed in Table 4. The NBO analysis of the studied stable A3-AT/GC stacked complex reveals that the $LP(1)O_5 \rightarrow \sigma^*H_{65}$-$N_{71}$ (AT) and $LP(1)N_{72} \rightarrow \sigma^*N_{64}$-$H_{82}$ (GC) transitions enhance the overall stability of the complex with maximum values of E^2 energy values *i.e.*, 16.86 and 14.26 kcal/mol respectively. Therefore, by interpreting the NBO data, we gain insights into the dynamics of charge transfer within both the unstacked A3 along with stacked A3-AT/GC systems. Additionally, we have conducted a similar analysis of charge transfer for the AT/GC base pairs as presented in Table 4.

Frontier Molecular Orbital (FMO) analysis

The analysis of Frontier Molecular Orbital (FMO) is a useful computational technique to determine numerous molecular properties including molecular reactivity, its ability to absorb light and encompassing both optical and electronic characteristics. This analysis is often used to determine the band gap of a molecule, which is calculated as the difference in energy between the highest occupied molecular orbital (HOMO) and the lowest unoccupied molecular orbital (LUMO). The fundamental property of this analysis is to assess and characterize the electronic structure of a molecule, which in turn can provide valuable insights into the molecule's pharmacological activity. This HOMO-LUMO study typically provides detailed explanation of the molecular reactivity, their stability and other electronic features such as charge transfer and interactions between agent-DNA systems. A large band gap indicates a significant energy difference between the HOMO and LUMO. This typically means that the molecule is less likely to participate in charge transfer interactions and is considered "hard." Hard molecules have a relatively low polarizability because it requires a substantial amount of energy to promote an electron from the HOMO to the LUMO. The lower band gap signifies the presence of charge transfer interactions within a molecule, which play a vital role in determining the bioactivity a molecule[35]. The polarizability of hard molecules is not higher than that of soft ones because hard molecules demand a significant amount of energy for excitation. Chemical hardness (η) is a measure of stability; higher chemical hardness indicates greater stability, while lower chemical hardness indicates greater reactivity. There are various intriguing characteristics of these parameters connected to the optimized metal complexes and AT/GC stacked systems which are displayed in Table 5 and Table 6. The hardness value of the most stable stacked A3-GC base pair complex has been determined as 0.011 eV, which is relatively lower in compared to its individual agent, A3 (η = 0.029 eV); Moreover, when evaluating the η values for the A3 complex in AT and GC base pairs, it ranges from 0.006-0.011 eV. These findings collectively indicate that the complex formed between the anticancer agent and DNA shows better reactivity in comparison to the individual systems as displays in Table 5 and Table 6.

However, the A3-AT/GC complex exhibits a lower chemical hardness value of 0.011 eV and higher chemical softness value at 88.81 eV^{-1}; these results suggest that the complex is comparatively softer than

Table 4 — Computed NBO analysis for the most favoured anticancer agent A3, $[Zn(Hnor)(Phen)(NO_3)_2]$ with AT/GC base pairs before and after complex formation with E^2 energie

Anticancer agent (A3)		Stacked A3 with AT/GC base pairs	
	E^2(kcal mol^{-1})	AT	E^2(kcal mol^{-1})
$LP^*_{(1)}C_{39} \rightarrow \sigma^*C_{37}$-$N_{49}$	168.21	$LP_{(1)}O_5 \rightarrow \sigma^*H_{65}$-$N_{71}$	16.86
π^*C_{19}-$C_{20} \rightarrow \pi^*C_{21}$-$C_{22}$	116.67	$LP_{(2)}O_{68} \rightarrow \sigma^*_{(1)}N_{66}$-$H_{67}$	7.93
$LP_{(1)}C_{24} \rightarrow \pi^*C_{21}$-$C_{22}$	48.13	$BD_{(3)}N_{64} \rightarrow \sigma^*C_{55}$-$H_{78}$	3.38
$LP_{(43)}O_2 \rightarrow LP_{(6)}^*Zn_1$	19.17	$LP_{(1)}O_5 \rightarrow \sigma^*_{(1)}C_{55}$-$H_{78}$	2.80
		GC	
$LP_{(2)}O_5 \rightarrow LP_{(2)}^*N_4$	211.76	$LP_{(1)}N_{72} \rightarrow \sigma^*N_{64}$-$H_{82}$	14.26
$\sigma^*_{(1)}O_{69}$-$C_{71} \rightarrow \pi^*N_{72}$-$C_{74}$	134.94	$LP_{(2)}O_{66} \rightarrow \sigma^*H_{67}$-$N_{70}$	12.26
$LP_{(3)}O_7 \rightarrow LP_{(6)}^*Zn_1$	74.08	$LP_{(1)}O_{66} \rightarrow \sigma^*H_{67}$-$N_{70}$	5.34
πN_{72}-$C_{74} \rightarrow \sigma O_{69}$-$C_{71}$	34.47	$LP_{(1)}O_5 \rightarrow \sigma^*C_{55}$-$H_{78}$	3.79

σ : Bonding orbital, σ *: Anti-bonding orbital, LP: Lone pair

Table 5 — Computed chemical reactivity parameters for optimized metal complexes

Agent-DNA complex	Chemical potential(μ)	Chemical hardness(η)	Softness(s)	Electrophilicity index(ω)
A1	–0.79	0.091	11.05	3.48
A2	–0.39	0.009	109.05	8.13
A3	–0.73	0.029	34.07	9.14

Table 6 — Computed chemical reactivity parameters for minimized stacked complexes

Agent-DNA complex	Chemical potential(μ)	Chemical hardness(η)	Softness(s)	Electrophilicity index(ω)
A1-AT	–0.56	0.041	24.64	3.83
A1-GC	–0.56	0.029	35.01	5.52
A2-AT	–0.59	0.019	53.56	9.21
A2-GC	–0.60	0.014	69.98	12.75
A3-AT	–0.67	0.007	149.03	33.35
A3-GC	–0.67	0.011	88.81	20.17

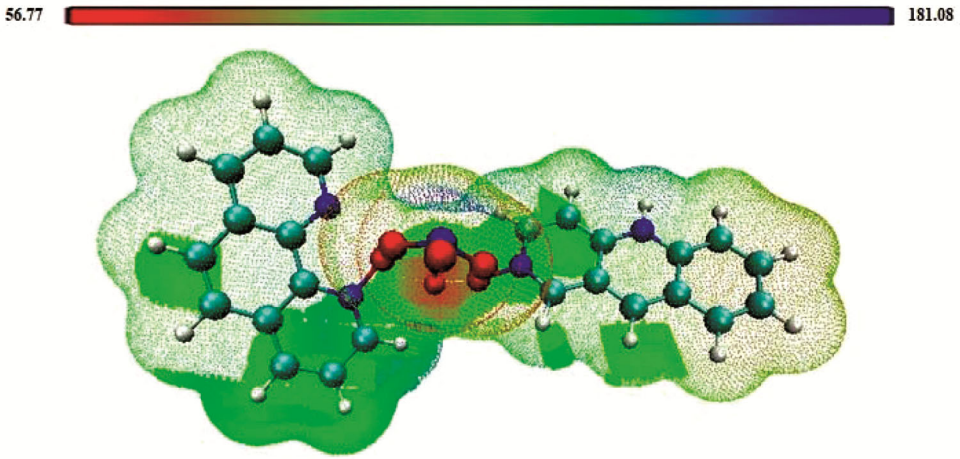

Fig. 4 — MEP surface of A3 unstacked system

its unstacked agent, A3. Further, the agent-DNA complex reveals an extremely higher electrophilicity index at 20.17 eV, which is significantly greater than the unstacked agent, A3 recorded at 9.14 eV. This observation indicates that the stacked A3 complex functions as an effective electrophile. The combination of a relatively low η value (0.011 eV) and a higher negative value of μ (–0.674 eV) signifies that the complex exhibits a high degree of polarizability. Thus, the above analysis substantiates the stability of the A3-AT/GC stacked complex, primarily due to its negative chemical potential value, which is calculated to be –0.674 eV. This stability is notably superior when compared to the A1 and A2 agents in associated with their stacked models of DNA base pairs as presented in Table 6.

Molecular electrostatic potential (MEP) analysis

The molecular electrostatic potential of a molecule serves as a valuable tool for understanding a range of properties, encompassing size and their dipole moment with density of electrons, hydrogen bonding interactions as well as chemical reactivity. In this visualization, different colours are used to represent specific characteristics of the molecular surface, where, red signifies electron-rich regions indicating a partially negative charge which is typically found around oxygen atoms which signifies them susceptible to electrophilic attack. Blue represents electron-poor areas with a partially positive charge which is distributed across the molecular system particularly around the hydrogen atoms making them prone to nucleophilic attack. Light blue denotes slightly electron-deficient regions, while yellow indicates slightly electron-rich domains. Green colour represents the neutral charge locations. The electrostatic potential map for the molecule in question was generated using the B3LYP/6-311G(d,p) method, which is displayed in Fig. 4 with the colour-coded representation.

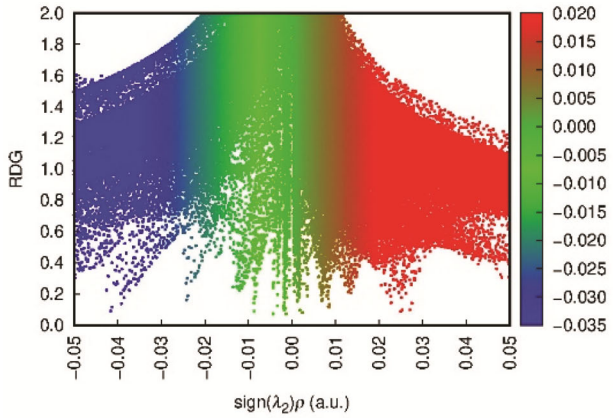

Fig. 5 — Non-covalent interaction (NCI) plots of the minimized models of A3-AT/GC stacked systems

Non-Covalent Interaction (NCI), Visual Molecular Dynamics (VMD) and Electron Localized Function (ELF) analysis

The analysis of non-covalent interactions (NCI) and reduced density gradients (RDG) provides a powerful tool for visually representing interacting regions within complex systems, aiding in the identification of specific interaction sites. As seen in Fig. 5, the NCI plots show spikes at low RDG densities which predicts nature of interactions within molecular complexes.

The NCI-RDG plot is generated by mapping the reduced density gradient in space, highlighting regions where attractive or repulsive forces occur. It identifies areas of significant interaction between molecules where, the attractive interactions are typically represented by blue regions, indicating regions where electrons are concentrated; while repulsive interactions are denoted by red regions, signifying areas of electron depletion. The plot helps to understand the nature and strength of weak interactions, contributing valuable information to the overall understanding of molecular structures and their behaviour. In this context, green colour indicates weak van der Waals interactions; blue signifies hydrogen bonding and red represents steric interactions. In this analysis, it's observed that van der Waals interactions dominate in both AT and GC base pair systems. For anticancer agent A1, the stacked-AT complex displays stronger van der Waals interactions compared to the stacked-GC system. Conversely, for A2, the stacked-GC complexes exhibit more dominant van der Waals interactions over the stacked-AT complex. However, A3 is unique among the metal-based anticancer agents as it maintains consistent van der Waals interactions in both AT and GC stacked systems as depicted in Fig. 5.

Again, Visual Molecular Dynamics (VMD) analysis is a useful tool in the field of molecular dynamics and computational chemistry. It is extensively used for the visualization, analysis and interpretation of complex systems. VMD allows to explore dynamic processes in biological molecules by providing an interactive 3D representation of molecular structures and their trajectories which reveals weak van der Waals interactions (green patches) between the anticancer agents and AT/GC base pairs. The bluer regions denote stronger attractive interactions, which may result from weaker hydrogen bond interactions. Red patches indicate van der Waals interaction regions, characterized by low electron density which is clearly presented in Fig. 6.

Density-based descriptions of chemical bonding, including the electron localization function (ELF) and the localized orbital locator (LOL) are important tools for understanding the nature of chemical bonds and electron distribution in molecules. These descriptors rely on topological methods and are built around the concept of the kinetic-energy density (τ), which reflects the reduction in quantum kinetic energy when orbitals are shared, a fundamental driving force behind covalent bonding. ELF is based on the consideration of electron pair density and it provides insights into the localization of electron pairs within a molecule. On the other hand, LOL recognizes that the gradients of localized orbitals are maximized when these orbitals overlap, helping to identify regions of electron localization and covalent bonding. These descriptors offer valuable tools for understanding the nature of chemical bonds and electron distribution in

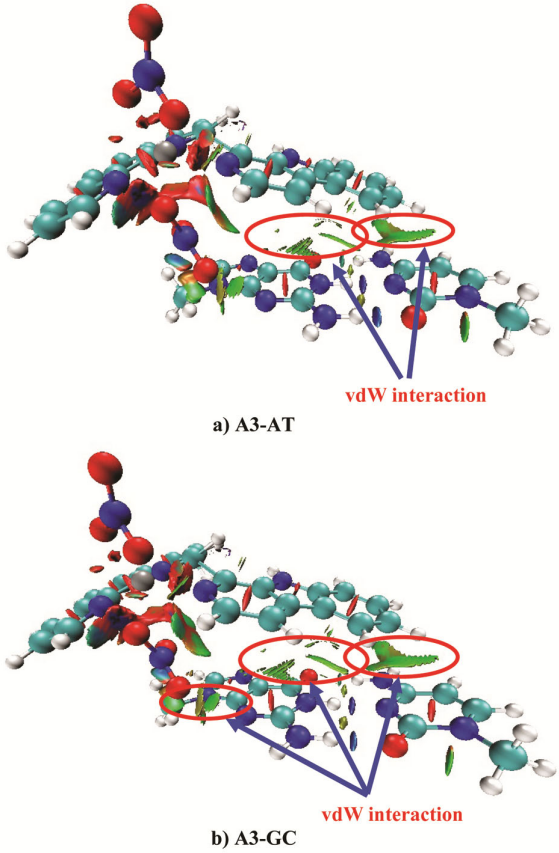

Fig. 6 — Visual molecular dynamics (VMD) models of the minimized models of A3-AT/GC stacked complexes

molecules. The topological analysis of electron localization functions (ELF) is used to describe chemical bonds mathematically. The 2D visualization of ELF isosurfaces for selected metal-based complexes demonstrates strong electronic localization in red and orange colours. A blue circle represents a depletion zone between valence and inner shells. Topological parameters of Electron Localization Descriptors are derived from ELF studies (as presented in Fig. 7), which further enhances the chemical concepts. Therefore, these comprehensive analyses and visualizations help us comprehend the intricate non-covalent interactions, electron localization and bonding properties within metal-based anticancer agents and their complexes with DNA. These insights contribute to a deeper understanding of the structural and chemical aspects of these systems.

Electrostatic Potential (ESP) and Becke Surface Analysis (BSA)

The quantitative analysis of molecular surfaces and Becke surface analysis reveal that the interaction

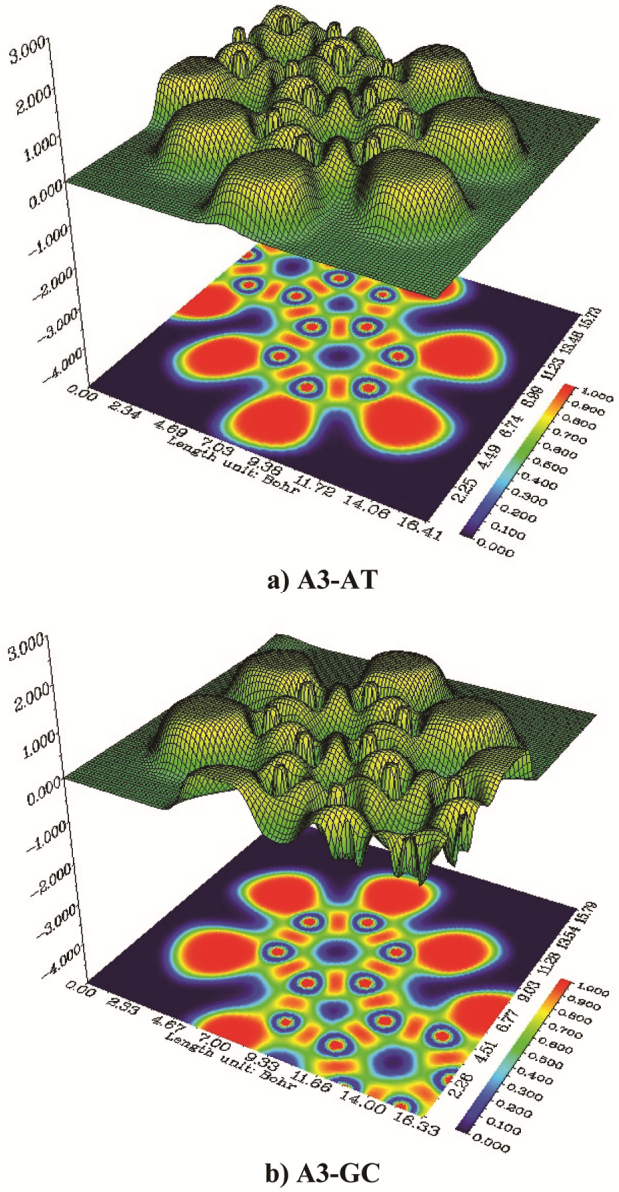

Fig. 7 — Electron localized function (ELF) plots of the minimized models of A3-AT/GC stacked systems

mechanisms of Zn^{+2} with DNA nucleobases involve electrostatic as well as hydrogen bonding interactions. The electrostatic potential (ESP) map provides the overall charge distribution map of a molecule which also identifies the reactivity of electrophilic or nucleophilic attacking sites. Based on the ESP values at various points on electron density isosurface regions; the red surface exhibits the least electrostatic (attractive) and the blue surface exhibits the most electrostatic (repulsive) potential energy values as illustrated in Fig. 8. Again, the isosurface has a Blue-White-Red (BWR) colour transition, which makes it

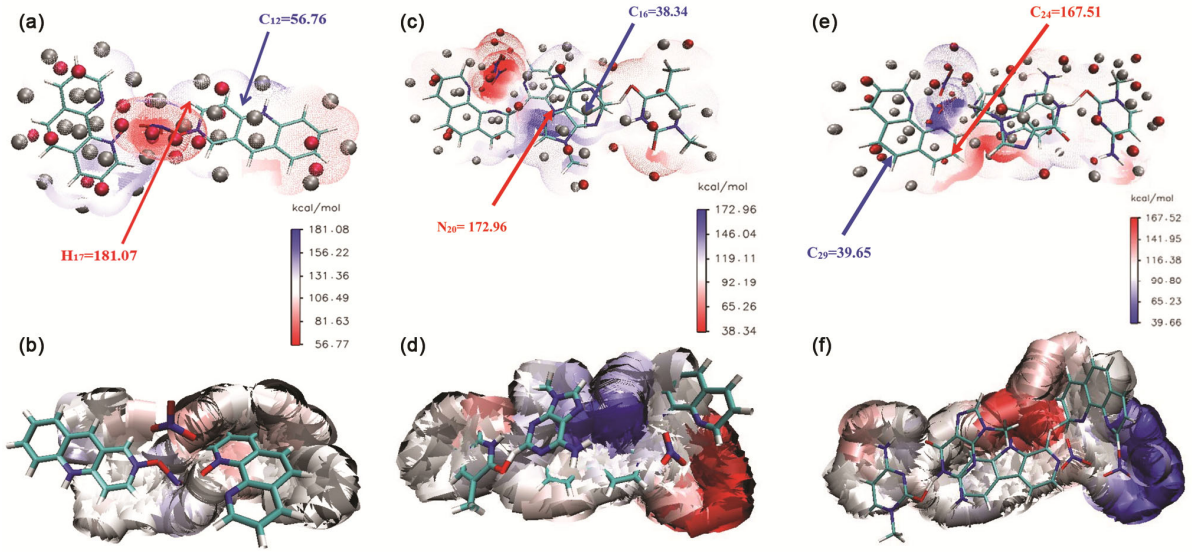

Fig. 8 — Electrostatic potential (ESP) diagrams of the minimized models of unstacked A3 and A3-AT/GC stacked systems

Table 7 — Electrostatic Potential analysis for the most favoured anticancer agent A3, $[Zn(Hnor)(Phen)(NO_3)_2]$ with AT/GC base pairs before and after complex formation with surface minima and maxima values

Anticancer agent (A3)		Stacked A3 with AT/GC base pairs	
	kcal/mol	AT	kcal/mol
C_{12}	56.76	C_{16}	38.34
H_{17}	181.07	N_{20}	172.96
		GC	
C_{12}	56.76	C_{29}	39.65
H_{17}	181.07	C_{24}	167.51

easy to identify the interaction region by merely observing the colours. The blue region implies favourable sites for electrophilic and radical reactions, red region implies favourable sites for nucleophilic reaction and white region represents the region between the two extremes *i.e.*, red and blue as depicted in Fig. 8. Herein, we get the surface minima and maxima values depending on the interacting regions. Where, surface minima indicate the best potential targets for electrophilic attack; and surface maxima value will function as a suitable site for nucleophilic attack by donating the hydrogen bond attached to it. Specifically, they can indicate regions of electron-rich (negative) or electron-poor (positive) charge density, which is crucial in understanding chemical bonding, reactivity and molecular properties. The surface maxima and minima atoms are shown in silver and red spheres of the ESP map generated with VMD software. In case of the A3 *i.e.*, the unstacked molecule, the colour scale of the map extends from 56 to 182 kcal/mol as cited in Fig. 8; whereas, in A3-AT stacked system, the colour scale on the map extends from 38 to 177 kcal/mol; similarly, for A3-GC system, the colour scale on the map extends from 39 to 168 kcal/mol. For A3 molecule, the carbon atom (C_{12}) having a lower value such as 56.76 kcal/mol is the surface minima and hydrogen atom (H_{17}) contains a higher value which is found to be 181.07 kcal/mol is the surface maxima. In A3-AT complex, the carbon atom (C_{16}) having a least positive value of 38.34 kcal/mol at surface minima by making it a favourable site for interaction; which can act as a target site for electrophilic attack; while the nitrogen atom (N_{20}) has the higher value of 176.08 kcal/mol which represents the surface maxima and functions as a hydrogen bond donor group as shown in Fig. 8. Similarly, in A3-GC complex, both surface maxima and minima have been found only for carbon atoms; the surface minima at C_{29} position having a lower value (*i.e.*, 39.65 kcal/mol) can behave as a hydrogen bond donor group which also represents as an electrophilic site while surface maxima at C_{24} position having a higher value (*i.e.*, 167.51 kcal/mol) can function as nucleophilic site as depicted in Table 7 and Fig. 8. However, the unstacked molecule is found

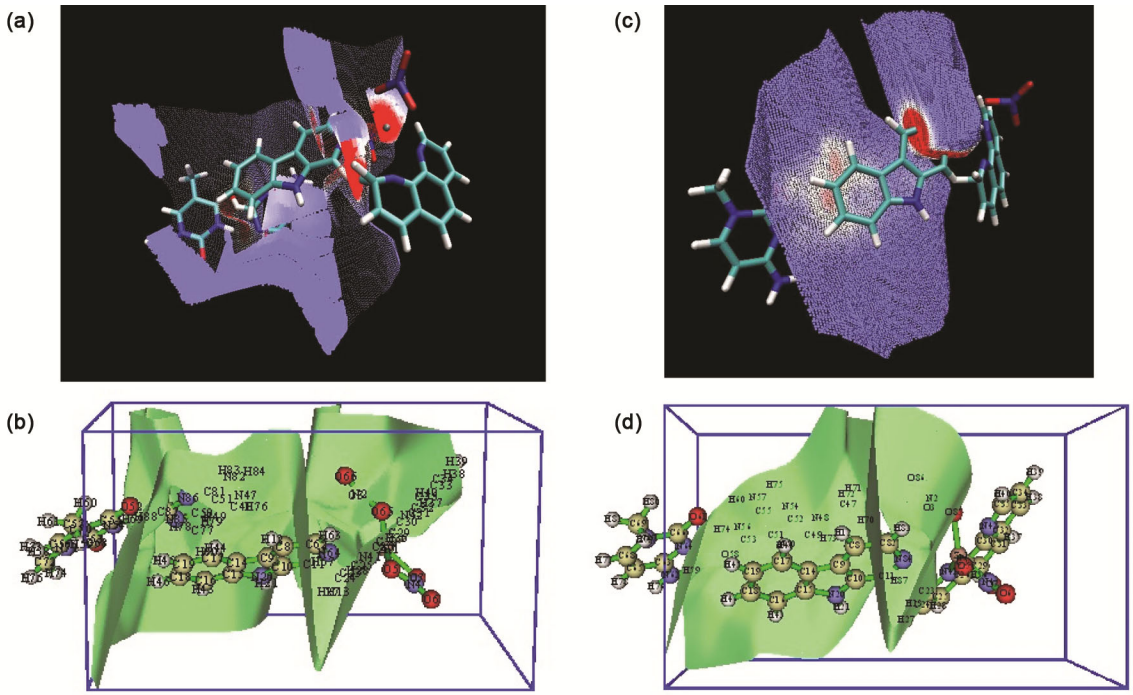

Fig. 9 — Becke surface analysis (BSA) diagrams of the minimized models of A3-AT/GC stacked systems

to be having more surface minima and maxima values in comparisons to the stacked complexes. It happens because of the distribution of electron density and nature of the electrostatic interaction exists between the molecular counterparts. Thus, in electrostatic potential analysis the presence of intermolecular interaction, charge density redistribution, symmetry and molecular geometry contributes to the observed differences in the number of minima/maxima values between unstacked and stacked systems. Therefore, stacked complexes tend to exhibit a more uniform electrostatic potential nature, leading to less prominent maxima and minima values compared to the isolated molecule.

Besides, the quantitative analysis of ESP, we further study the Becke surface analysis tool which may frequently used to identify the active site of an anticancer agents and also determine the relative intensity of interaction between metal ion and DNA nucleobases. As shown in Fig. 9, the Becke surface map for the most preferred Zn^{+2}-DNA base pair stacked system was coloured according to their electron density value (ρ). The Becke surface is represented by points and the presence of red zones corresponds to high electron density regions. The redder the colour of the Becke surface map, the higher the electron density. The red zones involve the interacting groups between Zn^{+2} complexes with AT/GC stacked systems, indicating that the complex A3-AT/GC may establish hydrogen bonds. The data range of the active sites between the interacting agents A3-DNA base pairs is shown in Fig. 9. In A3-AT stacked system, there are several interacting sites (red zones) between anticancer agent A3 and AT base pair *i.e.*, H_{46}-N_{64}, H_{45}-O_{61}, N_{56}-H_{45}, H_{71}-O_{86}, *etc*. where the relative intensity is ranges from 0.0031-0.355 a.u. Similarly, for A3-GC stacked system, the presence of interacting sites between drug-DNA are H_{59}-O_{58}, O_{61}-H_{45}, H_{70}-N_{84}, H_{70}-O_3, *etc*., where the relative intensity ranges from 0.022-0.482 a.u. Thus, formation of the red zones represents the sites where the interaction exists between anticancer agent-DNA nucleobases.

Cytotoxicity of metal complexes

Cytotoxicity of any metal complexes has been analysed based on their IC_{50} values. The literature revealed that the cytotoxic data for A1 complex exhibited more potency than the standard *cis*-platin towards T-24 cell line. The Mn^{+2} complex *i.e.*, A1 was evaluated against HepG-2 cell line; the IC_{50} value of Mn^{+2} complexes is found to be 11.03μM, hence the complex A1 was cytotoxic towards HepG-2 cell line. However, complex A2 is found to be the quite

effective towards all cancerous cells as it shows the most selectivity towards T-24 cell line with IC_{50} value of 7.04 ± 0.06μM. Again, the A3 complex containing norharmane and 1,10 phenanthroline ligand results in better cytotoxicity as the experimental cytotoxic data (1.26±0.07μM) reveals that metal complexes with phenanthroline ligand shows more cytotoxicity than any other ligands (Table 2). The complex has also shown greater potency than standard anticancer agent *cis*-platin towards T-24 cell line[32]. Drug potency, *i.e.*, the amount of drug required to produce an effect, is related to the IC_{50} value. Consequently, lower IC_{50} value represents more potential anticancer agents; if we compare the IC_{50} values of the above studied metal complexes we observe the following sequence of cytotoxicity:

A3 < A2 < A1

Thus, we could conclude that A3 metal complex having the least IC_{50} value is one of the potential and effective anticancer agents as compared to the other metal complexes.

Conclusion

From the above computational analysis, it has been explored that the pyridyl moiety based Mn^{+2}, Co^{+2} and Zn^{+2} metal complexes interact efficiently with DNA nucleobases through an intercalation mechanism. Among all the stacked agents, the interaction energy of A3 *i.e.*, $[Zn(Hnor)(Phen)(NO_3)_2]$ results relatively higher negative I.E. value *i.e.*, –25.56 kcal/mol, as compared to A1 and A2 stacked systems; hence, the stacked A3 complex appears as highly favourable to interact within DNA base pairs. Contrary to that, Mn^{+2}-based (A1) stacked anticancer agent $[Mn(QA)Cl_2]$, shows the minimum negative stacking interaction energy value of –10.63 kcal/mol; which clearly indicates that A1 shows weaker non-covalent interaction towards the DNA target sites. However, in A2 *i.e.*, $[Co(HClQ)_2(Py)_2]$, the computed interaction energy is found to be moderate (–19.58 kcal/mol) in comparison with A1 and A3; it arises as the interaction occurs only through the smaller pyridyl ligand rather than the bulky HClQ ligand. This stability order is further justified by the Irving-Williams series with experimentally determined stability constant for the high-spin complexes of the M^{+2} ions. In addition, the above analysis and comparison studies of changes which occur in Mulliken charge densities of M^{+2} ions for both stacked and unstacked models of these agents reveal the probable interacting sites within a stacked complex. Again, the variation observes in electronic transition which occurs in specific atom, bond pair or lone pair system of a stacked molecular entity can be justified by NBO analysis. Moreover, the above studies may be validated by visualization of the minimized models by analyzing NCI-RDG, VMD, ELF as well as ESP and BSA; such graphical model diagrams for the most favoured A3-DNA stacked system clearly ensure the possible non-covalent interaction sites, changes in electron charge densities, attractive and repulsive regions, electrophilic and nucleophilic target sites as well as their proper mode of interactions within DNA nucleobases.

References

1 Zhong Y, Jia C, Zhang X, Liao X, Yang B, Cong Y, Pu S & Gao C, *E J Med Chem*, 194 (2020) 112.
2 Monro S, Colon K L, Yin H, Roque III J, Konda P, Gujar S & McFarland S A, *Chem Rev*, 119 (2018) 797.
3 Murray B S & Dyson P J, *Curr Opin Chem Biol*, 56 (2020) 28.
4 Lu L P, Suo F Z, Feng Y L, Song L L, Li Y, Li Y J & Wang K T, *Eur J Med Chem*, 176 (2019) 1.
5 Leoni E, Mohanraj J, Holler M, Mohankumar M, Nierengarten I, Monti F, Sournia-Saquet A, Delavaux-Nicot B, Nierengarten J-F & Armaroli N, *Inorg Chem*, 57 (2018) 15537.
6 Nandanwar S K & Kim H J, Chem Sel, 4 (2019) 1706.
7 Vijayarohini P, Kavitha G, Alwar S B S & Swamidoss C M A, *Mat Today Proc*, 33 (2020) 4198.
8 Salman W A, *IJDDT*, 11 (2021) 123.
9 Rosenberg B, Camp L V, Trosko J E & Mansour V H, *Nature*, 222 (1969) 385.
10 Tabrizi L, McArdle P, Erxleben A & Chiniforoshan H, *Eur J Med Chem*, 103 (2015) 516.
11 Wang W, Vellaisamy K, Li G, Wu C, Ko C N, Leung C H & Ma D L, *Anal Chem*, 89 (2017) 11679.
12 Tabassum S, Zaki M, Ahmad M, Afzal M, Srivastav S, Srikrishna S & Arjmand F, *Eur J Med Chem*, 83 (2014) 141.
13 Yadav A A, Patel D, Wu X & Hasinoff B B, *J Inorg Biochem*, 126 (2013) 1.
14 Betanzos-Lara S, Chmel N P, Zimmerman M T, Barron-Sosa L R, Garino C, Salassa L, Rodger A, Brumaghim J L, Gracia-Mora I & Barba-Behrens N, *Dalton Trans*, 44 (2015) 3673.
15 Betanzos-Lara S, Gómez-Ruiz C, Barrón-Sosa L R, Gracia-Mora I, Flores-Álamo M & Behrens N B, *J Inorg Biochem*, 114 (2012) 82.
16 Barone G, Terenzi A, Lauria A, Almerico A M, Leal J M, Busta N & Garcia B, *Coord Chem Rev*, 257 (2013) 2848.
17 Sukanya P & Reddy C V R, *J Biomol Struct Dyn*, 40 (2021) 1.
18 Abdolmaleki S, Ghadermazi M & Aliabadi A, *Inorg Chim Acta*, 527 (2021) 120549.
19 Zhang A L, Li X C, Min J, Tan L T, Xu H L, Zhu X G & Yang J, *Inorg Chim Acta*, 522 (2021) 120.

20 Regino C A S, Torti S V, Ma R, Yap G P A, Kreisel K A, Torti F M, Planalp R P & Brechbiel M W, *J Med Chem*, 48 (2005) 7993.
21 Long E C & Barton J K, *Acc Chem Res*, 23 (1990) 271.
22 Reedijk J, Wilkinson G, Gillard R D & McCleverty J A (Eds.), *Comprehensive Coordination Chemistry*, Vol 2, (Pergamon, Oxford) 1987, p 73.
23 Hoque M A, Chowdhury A D, Maji S, Benet-Buchholz J, Ertem M Z, Surinach C G, Lahiri G K & Llobet A, *Inorg Chem*, 60 (2021) 5791.
24 Chen Y, Qin M Y, Wu J H, Wang L, Chao H, Ji L N & Xu A L, *Eur J Med Chem*, 70 (2013) 120.
25 Lou X W, Buijtenen J V, Bastiaansen J, Waal B F M D, Langeveld B M W & Dongen J L V, *Mass Spect*, 40 (2005) 654.
26 C P Tan, Wu S H, Lai S S, Wang M X, Chen Y, Zhou L J, Zhu Y P, Lian W, Peng W L, Ji L N & Xu A L, *Dalton Trans*, 40 (2011) 8611.
27 Khan R A, Al-Farhan K, Almeida A D, Alsalme A, Casini A, Ghazzali M & Reedijk J, *Inorg Biochem*, 140 (2014) 1.
28 Mohamadou, Albada G A V, Mutikainen I, Turpeinen U, Marrot J & Reedijk J, *Polyhedron*, 28 (2009) 2813.
29 Reedijk J, *Eur J Inorg Chem*, 10 (2009) 1303.
30 Reedijk J, *Chem Soc Rev*, 42 (2013) 1776.
31 Agarwal P, Asija S, Deswal Y & Kumar N, *J Indian Chem Soc*, 99 (2022) 100.
32 Lan X, Liu T, Wang Z, Govorov A O, Yan H & Liu Y, *J Am Chem Soc*, 140 (2018) 11763.
33 Frisch M J, Trucks G W, Schlegel H B, Gill P M W, Johnson B G, Robb M A, Cheeseman J R, Keith T, Petersson G A, Montgomery J A, Raghavachari K, Al-Laham M A, Zakrzewaki V G, Ortiz J V, Foresmann J B, Ciolowski J, Stefanov B B, Namayakkara A, Challacombe M, Peng C Y, Ayala P Y, Chen W, Wong M W, J L Andres, Replogle E S, Gomperts R, Martin L R, Fox D J, Binkley J S, Defrees J, Baker J, Stewart J P, Head-Gordon M, Gonzalez C, Pople J A, *Gaussian*, (Gaussian Inc., Pittsburgh PA) 2003.
34 Reed A E, Weinstock R B & Weinhold F, *J Chem Phys*, 83 (1985) 735.
35 Benzir A, Pratyashee B, Mrinal B, Ibrahim A & Bipul B, *J Indian Chem Soc*, 99 (2022) 100391.
36 N Chipanina, *Tetrahedron*, 70 (2016) 1207.
37 Parthasarathi R, *Bioorg Med Chem*, 12 (2004) 5533.
38 Vargas R, Garza J & Cedillo A, *J Phys Chem A*, 109 (2005) 8880.
39 Chattaraj P K & Giri S, *Annu Rep Prog Chem Sect C: Phys Chem*, 105 (2009) 13.
40 Benzir A, Pratyashee B & Bipul B, *J Indian Chem Soc*, 100 (2023) 101027.
41 Humphrey W, Dalke A & Schulten K, *J Mol Graph*, 14 (1996) 33.
42 Tian L & Feiwu C, *J Comp Chem*, 33 (2012) 580.
43 Silvi B & Savin A, *Nature*, 391 (1994) 683.
44 Noureddine O, Issaoui N, Medimagh M, Al-Dossary O & Marouani H, *J King Saud Uni- Sci*, 33 (2021) 101334.
45 Janani S, Rajagopal H, Muthu S, Aayisha S, Raja M & Irfan A, *Heliyon*, 7 (2021) e08186.
46 Zhang J & Lu T, *Phys Chem Chem Phys*, 23 (2021) 20323.
47 Lu T & Chen F, *J Mol Graph Model*, 38 (2012) 314.
48 Hosmane R S, *Prog Heterocyc Chem*, 21 (2019) 35.
49 Caterina B & Bernd K, *J Med Chem*, 53 (2010) 5061.
50 Timsit Y, *Int J Mol Sci*, 14 (2013) 8252.
51 Alotaibi S H & Momen A A, *Bio Phy Chem-Adv App*, (2020) 110. (https://doi.org/10.5772/intechopen.73426).
52 Irving H & Williams R J P, *J Chem Soc*, (1953) 3192. (https://doi.org/10.1039/JR9530003192).